A novel *in situ* electrochemical NMR cell with a palisade gold film electrode

Cite as: AIP Advances **7**, 085205 (2017); https://doi.org/10.1063/1.4997887
Submitted: 18 May 2017 • Accepted: 25 July 2017 • Published Online: 03 August 2017

Zu-Rong Ni, Xiao-Hong Cui, Shuo-Hui Cao, et al.

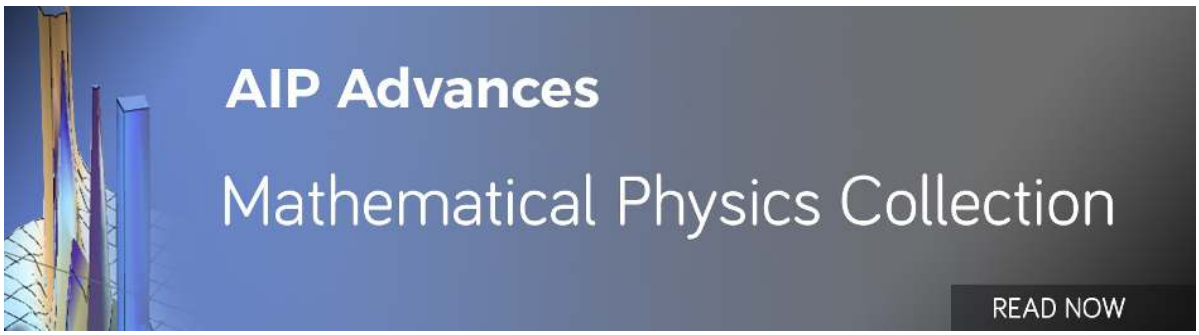

A novel *in situ* electrochemical NMR cell with a palisade gold film electrode

Zu-Rong Ni, Xiao-Hong Cui, Shuo-Hui Cao,[a] and Zhong Chen
Department of Electronic Science, Fujian Provincial Key Laboratory of Plasma and Magnetic Resonance, State Key Laboratory of Physical Chemistry of Solid Surfaces, Xiamen University, Xiamen, Fujian 361005, China

(Received 18 May 2017; accepted 25 July 2017; published online 3 August 2017)

In situ electrochemical nuclear magnetic resonance (EC-NMR) has attracted considerable attention because of its ability to directly observe real-time electrochemical processes. Therefore, minimizing the incompatibility between the electrochemical device and NMR detection has become an important challenge. A circular thin metal film deposited on the outer surface of a glass tube with a thickness considerably less than the metal skin depth is considered to be the ideal working electrode. In this study, we demonstrate that such a thin film electrode still has a great influence on the radio frequency field homogeneity in the detective zone of the NMR spectrometer probe and provide theoretical and experimental confirmation of its electromagnetic shielding. Furthermore, we propose a novel palisade gold film device to act as the working electrode. The NMR nutation behavior of protons shows that the uniformity of the radio frequency field is greatly improved, increasing the sensitivity in NMR detection. Another advantage of the proposed device is that an external reference standard adapted to the reaction compound can be inserted as a probe to determine the fluctuation of the physico-chemical environment and achieve high-accuracy quantitative NMR analysis. A three-chamber electrochemical device based on the palisade gold film design was successfully fabricated and the *in situ* electrochemical NMR performance was validated in a standard 5 mm NMR probe by acquiring voltammograms and high-resolution NMR spectra to characterize the electrochemically generated species. The evolution of *in situ* EC-NMR spectrum monitoring of the redox transformation between *p*-benzoquinone and hydroquinone demonstrates the ability of the EC-NMR device to simultaneously quantitatively determine the reactants and elucidate the reaction mechanism at the molecular level. [http://dx.doi.org/10.1063/1.4997887]

I. INTRODUCTION

Nuclear magnetic resonance (NMR) spectroscopy is a powerful method for structural analysis and dynamic investigation of chemical reaction systems. Combined with electrochemical (EC) methods, NMR can provide crucial insight into the processes at and near the electrode surface at the molecular level.[1–8] However, despite such promise, *in situ* EC-NMR spectroscopy is underused compared with other spectro-EC techniques, such as ultraviolet–visible and infrared spectroscopy.[9–11] This originates from the technical incompatibility between the indispensable electrical conductivity of the EC setup and the good detection of NMR signals. For example, introduction of asymmetric conductive electrodes into the NMR detection region has a strong influence on the homogeneity of the magnetic field, especially the radio frequency (RF) field, in the probe head. Furthermore, the

[a]E-mail: shuohuicao@xmu.edu.cn

uniform RF field $\hat{B}_1$ over the sample volume is a crucial premise of most NMR techniques developed for extracting structural or quantitative information about intermediates in EC-NMR experiments. Based on the so-called principle of reciprocity,[12] $\hat{B}_1$ is included in the equation

$$\xi = -\frac{d}{dt}(\hat{B}_1 \cdot M) \tag{1}$$

where ξ is the intensity of the time-varying voltage induced per unit sample volume across the received coil and $\boldsymbol{M}$ are the local values of the transverse rotating magnetic moment. Therefore, the spatial uniformity of ξ inside a homogeneous sample can be adversely affected by variation of the RF field amplitude and the distribution of its phase. These negative effects lead to a large decrease of the optimum performance of NMR in EC analysis. Generally, flip-angle errors in the observed and irradiated nuclei pulses will result in variation of the magnetization and insufficient decoupling efficiency, causing variation of the observed signal height and unfavorable resolution of the spectrum in multi-pulse decoupling experiments. Furthermore, non-uniform flip angles result in spatial uniformity of the NMR response in the specimen and inaccurate manipulation of spin operators through desired coherence-transfer pathways during multiple-pulse sequences, especially in multidimensional NMR spectroscopy for structural elucidation of the EC reaction products.

In situ studies have been performed with bulk electrodes directly located in the RF coils of the probe, but with varying degrees of success.[13–19] To avoid the inherent incompatibility between electrochemistry and NMR, a thin metal film has been used as a working electrode by several research groups to take advantage of the "skin depth" effect in the *in situ* EC-NMR cell. Mincey et al.[16] used a thin Sb–SnO_2 semiconductor film as the working electrode. Prenzler[18] and Webster[19] used a gold film deposited outside a glass tube as the working electrode. Compared with Sb–SnO_2 semiconductor films, metallic gold films perform at faster electrolysis rates. The abovementioned studies were all based on the hypothesis that the NMR RF field penetrates into the super thin metal film electrode without any loss when the film thickness is much smaller than the skin depth. However, comparison of dimethyl benzene-1,3-dicarboxylate NMR spectra obtained using EC-NMR cells with different Au electrode thicknesses shows that even if the electrode thickness is only 40 nm, which is much less than the skin depth, for the non-uniform RF field to still exist, the spectral resolution and intensity are notably reduced.[19] Consequently, a compromise has to be made and a thin Au film needs to be used, resulting in a weak electrolytic current and the film easily falling off the glass tube.

In this study, rather than using a fully coated thin film, we used a thin palisade gold film (PGF) electrode in the EC-NMR cell to make the electrolytic cell suitable for conventional operation with a modern high-field NMR spectrometer. The RF field uniformity in the detection area of the NMR probe was determined by both theoretical analysis and NMR nutation experiments. For the cell assembly, evolution of the *in situ* EC-NMR spectrum was used to monitor the redox behavior of *p*-benzoquinone and hydroquinone over time to determine the feasibility of the *in situ* EC-NMR technique.

II. EXPERIMENTAL

A. Reagents and instruments

All of the chemicals used for electrolysis were reagent grade and purchased from Sinopharm, including *p*-benzoquinone (99.5%), benzene (95%), 1,2-ethanediol (99%), 2-propanal (99.7%), and phenol (99%). Milli-Q water was used for preparation of the solutions for the experiments. All of the chemicals for nanoparticle preparation ($HAuCl_4$, $NaBH_4$, sodium citrate, and 3-aminopropyltrimethoxysilane (97%)) were purchased from Sigma-Aldrich. In the NMR experiments, deuterium oxide (99.8% D, Aldrich) was used to prepare the deuterated solutions. The ^{1}H NMR spectra were acquired with a 500 MHz spectrometer (Agilent Technologies, Santa Clara, CA) and the chemical shifts were aligned with respect to the signal of tetramethylsilane. According to test samples with low concentrations (<50 mM), the number of acquisition was 32 times, which kept each acquisition time less than 3 min.

The EC measurements were performed in a homemade EC-qNMR cell with a CHI631A potentiostat (Chenhua Co., China). The sweep rate was 50 mV/s. A Pt plate and Ag/AgCl wire electrode were used as the counter and reference electrodes, respectively. All of the potentials are with respect

to the Ag/AgCl electrode. The working electrode was constructed by depositing a PGF film with a thickness on the order of 50 nm on the outer wall of a 2-mm-(outer diameter) OD capillary. Prior to the EC measurements, the PGF electrode was processed by cyclic voltammetry cleaning in 0.1 M H_2SO_4. The solution was also deaerated by ultrapure nitrogen for 15 min prior to the measurements.

B. Design of the EC-NMR cell

The homemade electrolytic cell was fabricated from several different OD glass tubes, as shown in Fig. 1. Two 9-cm-long 10-mm-OD (a) and 5-cm-long 5-mm-OD NMR tubes (b) were spliced together by the heat fusion method to assemble the outermost compartment. The upper 10-mm-OD section conformed with the standard 10-mm-inner-diameter NMR holder (c), which also provided sufficient space to house the counter (d) and reference (e) electrodes. The lower 5-mm-OD section designed to embody the working electrode (f) was suitable for the common 5-mm probe of a conventional commercial liquid phase NMR spectrometer. Compared with a 10-mm probe, the increased filling factor of the coil could lead to a much higher signal to noise ratio (SNR) and shorter acquisition time.

A 2-mm-OD half-open capillary tube (g), whose outer wall was covered with a thin PGF film by the colloidal reduction method,[20] served as the working electrode and was coaxially located in the outermost lower section of the chamber, which was also in the central detectable area of the saddle coil of the NMR spectrometer probe. A Teflon enameled wire was stuck to the upper portion of the working electrode by conductive silver glue. An external reference standard adapted to the reaction compound can be chosen and poured into the capillary tube, whose open port is carefully sealed by

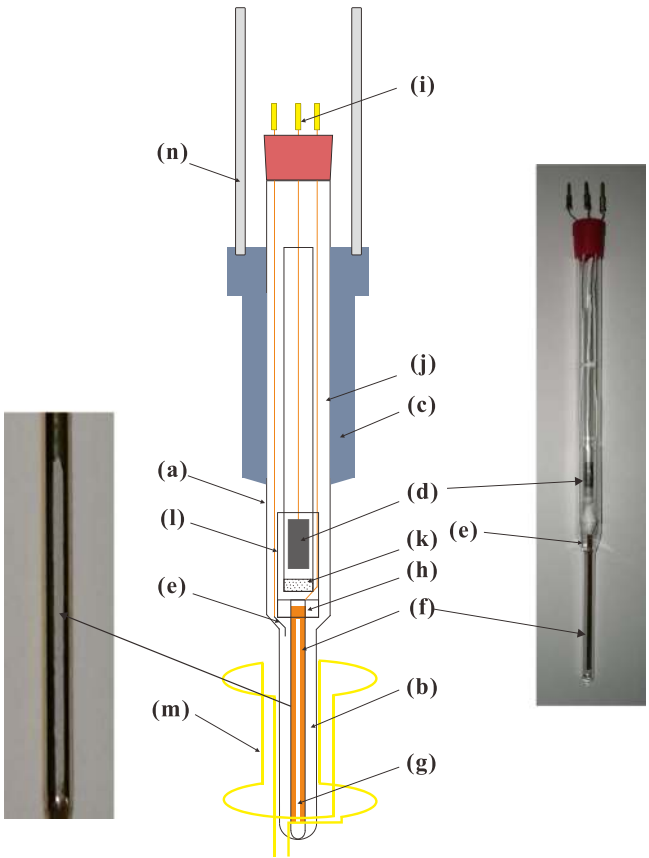

FIG. 1. Side view of the liquid phase EC-NMR cell. (a) 10-mm-OD NMR tube, (b) 5-mm-OD NMR tube, (c) NMR holder, (d) cylindrical platinum counter electrode, (e) Ag/AgCl reference electrode, (f) 50-nm-thick Au PGF working electrode, (g) 2-mm-OD capillary tube with external standard inside, (h) Teflon band, (i) male connector, (j) 5-mm-OD NMR tube for housing the counter electrode, (k) porous glass frit, (l) 7-mm-OD glass tube, and (m) saddle coil of the NMR probe.

a Teflon band (h) to prevent the external standard and silver glue from interfering with the reaction. Therefore, variation of the concentration of the EC reactants can be conveniently calibrated in real time.

The counter electrode, a 0.5-mm-diameter cylindrical black platinum plate linked to the gold-plated connector (i) with Teflon enameled wire, was placed inside another 5-mm-OD tube (j), which served as an auxiliary electrode reaction area and was sealed by porous glass frit (k) at its base to maintain the connection of the solution and prevent any byproducts generated at the auxiliary electrode from contaminating the main test solution at the working electrode.

To further isolate the auxiliary electrode from the working electrode, a 2-cm-long 7-mm-OD tube (l) acted as an additional compartment to house the 5-mm-OD tube. It was coaxially fixed outside the top of the 2-mm-OD capillary tube by a Teflon band. A customized 110-mm-long 1-mm-OD Ag/AgCl electrode was placed inside the gap between the 7-mm-OD and 10-mm-OD tubes as the reference electrode, and its end was located as close as possible to the working electrode for higher measurement precision of the electrical potential.

Three leading wires were drilled through the NMR tube cap and then soldered to male connectors. The interspaces between the wires and holes in the cap were filled with Teflon wrapping around the wires to keep the cell oxygen free. The EC-NMR cell was degassed in a conical flask by a vacuum pump and then purged with nitrogen. The deoxygenated solvent/solute was injected into the cell with an airtight syringe under a nitrogen atmosphere.

The assembled cell was then threaded through the inner bore of the NMR spectrometer by two cylindrical Delrin rods (n), which were attached to the upper section of the NMR holder and banded together with three coaxial cables soldered to the male connector. The RF chokes on the entrance of the bore were connected in series with coaxial cables to block mutual interference between the NMR spectrometer and the potentiostat through the connecting cables. The metallic shields of the cables should be well grounded at the side of the potentiostat to prevent electromagnetic interference from the surrounding environment.

III. RESULTS AND DISCUSSION

A. Reduced interference of the RF field

Classically, the penetration depth of a vertical incidence RF field into a metal plane (approximated by the skin depth, δ) is defined as the thickness of the conductor above which the amplitude of the RF radiation falls to e^{-1} (about 37%) of its surface value. It can be calculated by

$$\delta = (\rho/\pi\nu\mu_0)^{1/2} \tag{2}$$

where ρ is the electrical resistivity of the metal, υ is the RF field frequency, and μ_0 is the magnetic permeability. Usually, when the thickness of the metal plane Δ is much larger than the skin depth δ, it shows an excellent shielding effect in an alternating magnetic field.

Penetration of a magnetic field into a special shape, such as a cylinder or sphere, is not only determined by the skin depth δ. The theoretical analysis (see Fig. S1 in the supplementary material) shows that the applied field can be effectively screened even when the cylinder thickness is far less than the skin depth (e.g., 3.3 μm for gold at a frequency of 500 MHz). Fig. 2 shows that the time alternating magnetic field in an Au film cylinder with 2 mm diameter is shielded for film thicknesses of a few tens to a hundred nanometers. The spatial distribution of the magnetic field in a 100-mm-long Au film cylinder is shown in Fig. 3(a), where the intensity of the applied RF magnetic field along the *y* direction is 10^{-4} T. For comparison, mitigation of the applied RF magnetic field spatial distortion by a single thin film strip is shown in Fig. 3(b). The magnetic field induced by the eddy currents of the Au film strip at azimuth angles of 15°–45° in the same external applied magnetic field as Fig. 3(a) can almost be ignored. Improvement of the RF field homogeneity over the volume of the substances in the EC-NMR cell with a palisade structure of the working electrode based on a Au film strip is expected for a RF field that can penetrate into the strips without any interference. For the same reason, an external reference standard adapted to the reaction compound can be chosen and poured into the 2-mm-OD capillary tube for quantitative NMR (qNMR) analysis. The absolute content method for

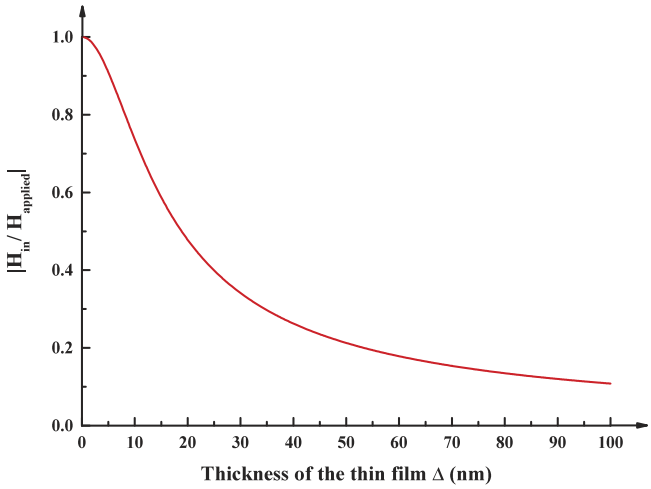

FIG. 2. Shielding of the time alternating magnetic field in 2-mm-OD Au film cylinders with different thicknesses. H_{in} is the magnetic field inside the cylinder and H_{applied} is the external applied magnetic field.

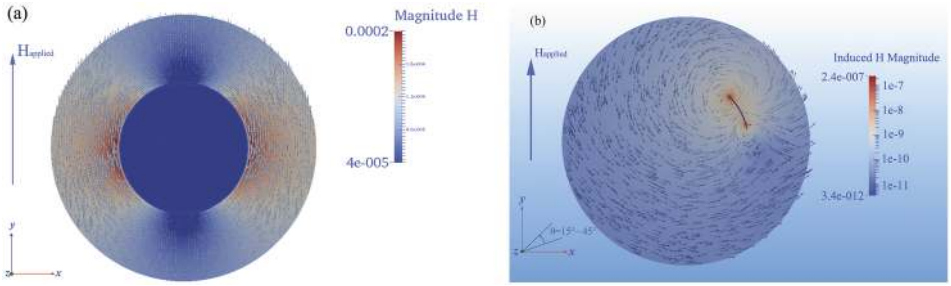

FIG. 3. (a) Spatial distribution of the magnetic field in a 100-nm-long Au film cylinder with diameter 2 mm. (b) Magnetic field induced by the eddy currents of a Au film strip along the z direction with the same thickness at azimuth angles θ 15° – 45°relative to the x axis. The applied RF magnetic field is along the y direction.

quantitative content determination in EC-NMR is given in the supplementary material, as well as its precision and accuracy.

The RF field uniformity for different structures of the working electrode was investigated by traditional one-dimensional (1D) NMR and nutation experiments. Fig. 4 shows the 1D NMR spectra of 0.5 M glycol in D_2O solution. The SNR in the EC-NMR cell with the PGF electrode is more than six times higher than that with the fully coated Au film, which means enhancement of the sensitivity in NMR detection. As shown in the insert of Fig. 4, even weak hump signal in conventional NMR spectra can reappear in the condition of PGF electrode, while disappear in the condition of fully coated Au film, which further demonstrate the advantage of PGF electrode to ensure the sensitivity of EC-NMR measurement. However, compared with the value of the SNR in the regular NMR tube, there is still some RF field uniformity because of mutual induction between the two strips. The resolutions of the spectra are 2.17, 2.31, and 2.69 Hz for 0.5 M glycol, the PGF electrode, and the fully coated Au film, respectively. The reason for such small differences in the resolutions is that there is little influence on the static field homogeneity when the main boundaries of the Au film are all along the direction of the applied static magnetic field.[21]

Nutation measurements were performed when the fully coated thin film electrode and PGF electrode were separately inserted into ethylene glycol solution by varying the pulse length of the single-pulse NMR experiment and recording the resulting signal amplitude. Fig. 5 shows the behavior of the nonconductive ethylene glycol standard with a naked 2-mm-OD capillary. The data are well characterized by a sine curve. The ratio of the amplitude of the signal following the 810° pulse to that of the 90° pulse reaches 80%, which is similar to that using only glycol. However, when the outer

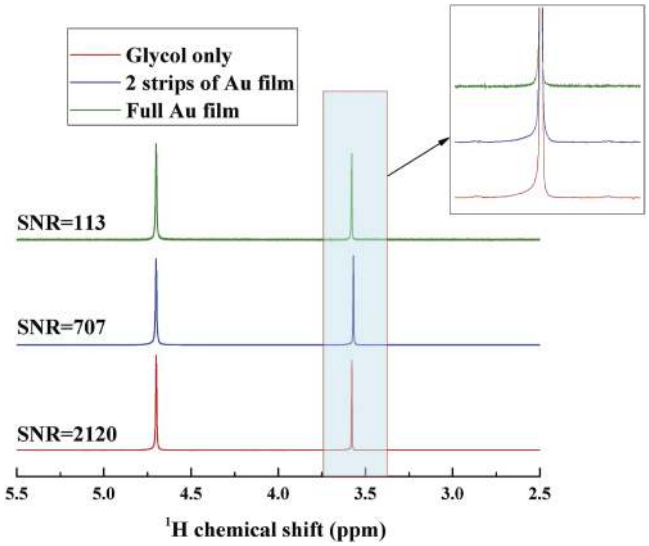

FIG. 4. NMR spectra of 0.5 M glycol in D_2O solution. The bottom spectrum was acquired in a regular NMR tube. The top two spectra were acquired in the EC-NMR cell with fully coated Au and PGF films, respectively. The SNR values are given beside each spectrum. The insert shows enlargements of the spectra with the same magnification. The peak at 4.7 ppm is the residual H_2O in D_2O.

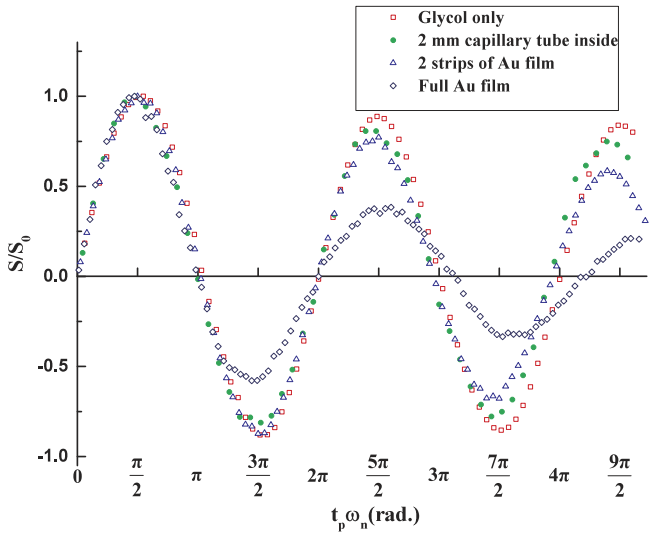

FIG. 5. Nutation behavior of ethylene glycol standard in the EC-NMR cell with different structures of the working electrode: only glycol (□), naked 2-mm-OD capillary (•), covered with two strips of Au film (△), and fully covered with Au film (◇).

surface of the capillary is fully covered by a Au film with a thickness of about 50 nm, which is much thinner than the Au skin depth at 500 MHz, the ratio decreases to 21%, which indicates destruction of the RF field uniformity by the Au film. The ratio of the two parallel symmetrical Au strips remaining after scraping off the redundant Au film along the axial direction of the capillary is nearly 60% and there is significant improvement in the RF homogeneity. This is because the magnetic lines of the force, rather than those surrounding the surface of the metal film, mostly penetrate into the capillary and thus a suitable external standard can be introduced into the capillary for quantitative analysis.

B. EC-NMR performance: *p*-benzoquinone

The well-known redox system of *p*-benzoquinone and hydroquinone was chosen to investigate the performance of our EC-qNMR system. The sample was 2.5 mM *p*-benzoquinone dissolved in

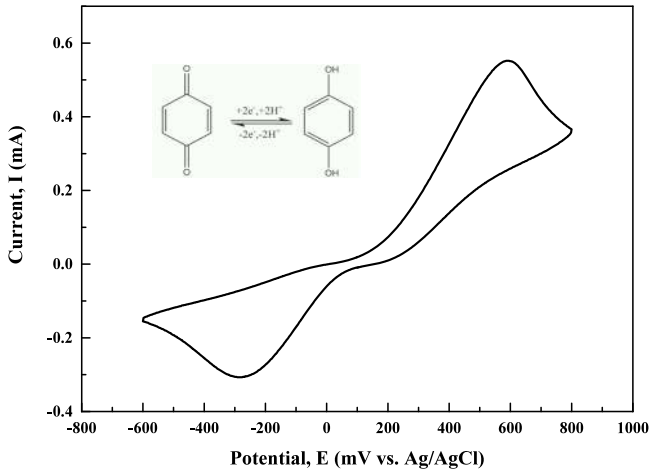

FIG. 6. Cyclic voltammogram of *p*-benzoquinone with a PGF electrode system in sulfuric acid solution.

0.1 M H_2SO_4, with 20 mM benzene poured into the capillary as the external standard. The sulfuric acid solvent acted as a proton donor to provide sufficient electron transfer during reduction of *p*-benzoquinone to hydroquinone. The *in situ* cyclic voltammogram of benzoquinone acquired inside the NMR probe is shown in Fig. 6. The first reduction potential is –300 mV (Ag/AgCl), while the reoxidation peak appears at +600 mV. A series of *in situ* NMR spectra was simultaneously collected during the EC reactions. Fig. 7(a) shows the NMR spectra recorded when the reduction reaction was performed at the potential of −300 mV. The NMR spectra of the four phenyl protons of benzoquinone and hydroquinone both consist of singlets, with slightly different chemical shifts of 6.89 and 6.82 ppm in sulfuric acid solution, respectively. The NMR spectra of the six phenyl protons of benzene also consist of singlets, with chemical shifts of 7.36 ppm. After several minutes of electrolysis, a distinctive proton signal peak indicating the reduction product hydroquinone appears at 6.82 ppm. With increasing electrolysis time, the general trends of an increase of the peak at 6.82 ppm and a decrease of the peak at 6.89 ppm show the evolution of production of hydroquinone and consumption of benzoquinone. After 40 min of electrolysis, the signal intensity at 6.89 ppm gradually decreases and the signal intensity at 6.82 ppm nearly reaches its maximum. The reason why it is difficult to completely exhaust the benzoquinone electrolyte is its slow diffusion down from the upper 7-mm-OD glass tube to the PGF working electrode. However, after a long electrolysis time, the signal peak at 6.89 ppm disappears and there is only one peak at 6.82 ppm. Oxidation of hydroquinone was then performed by applying a positive potential of 600 mV to the same solution and the NMR spectra were acquired (Fig. 7(b)). During the oxidation period, a peak appears at 6.89 ppm and then

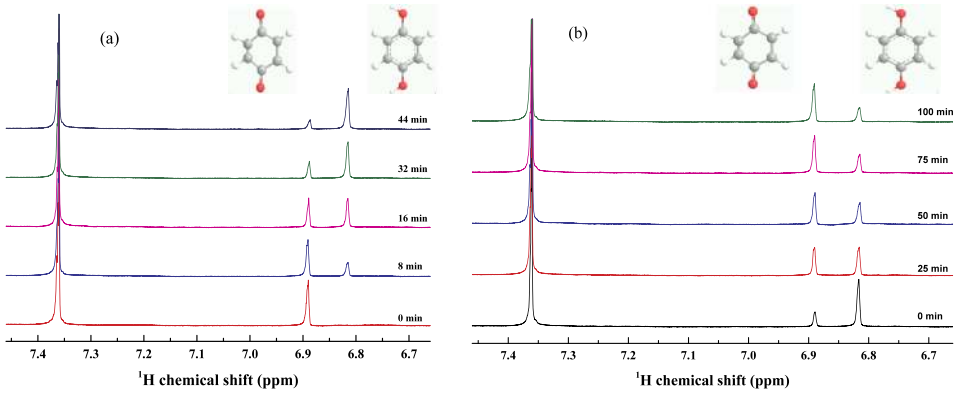

FIG. 7. NMR spectra of redox of *p*-benzoquinone during electrolysis in sulfuric acid solution at potentials of (a) −300 mV and (b) +600 mV.

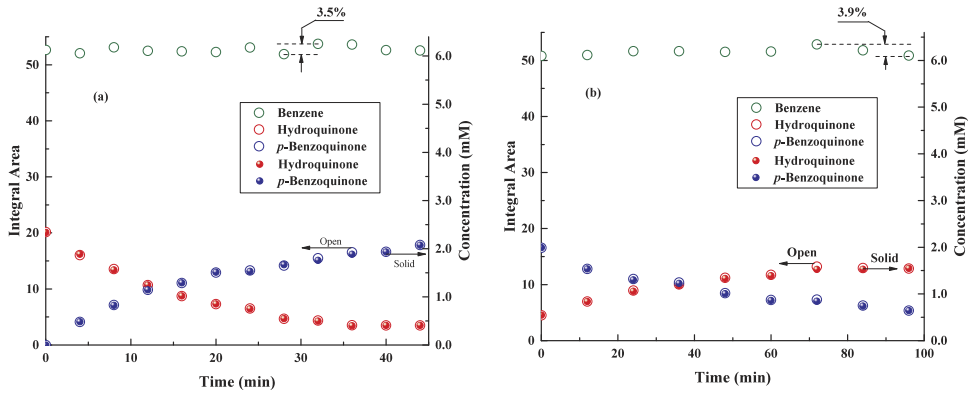

FIG. 8. Integral data from the ^{1}H NMR spectra and the change of amended concentrations of the species with experimental time during the EC-qNMR experiments. (a) Reduction of *p*-benzoquinone and (b) oxidation of hydroquinone: 20 mM benzene external standard (green open circles), *p*-benzoquinone (blue open circles), hydroquinone (red open circles), and amended concentrations of *p*-benzoquinone (blue solid circles) and hydroquinone (red solid circles).

gradually increases, and the peak at 6.82 ppm simultaneously decreases. With the EC-qNMR system, complete reduction of *p*-benzoquinone to hydroquinone and reoxidation to *p*-benzoquinone can be observed.

Fig. 8 shows the trends of the peak areas of benzene, *p*-benzoquinone, and hydroquinone in the reduction and reoxidation period of the double electron transfer EC reaction between *p*-benzoquinone and hydroquinone. The maximum peak area variation of benzene reaches about 3.9% even though it is isolated from the EC reagent in the capillary tube as an external standard. There are several factors that affect the quantitative precision and accuracy of peak area determination. Integration of the peak area is highly sensitive to the range of the integral region and distortion of the baseline. The integral region should be sufficiently extended in both directions to cover the majority of the peak area. Several slope and bias settings should be used to define the baseline in the integral region, and the average value of the integration areas should be chosen to reduce the analyst error.

The stability of the physico-chemical environment of the protons is also an important factor that affects the reproducibility of the quantitative results. During the electrolysis period, there are several experimental parameters that depend on the microenvironment of every proton. These factors deviate from their pre-calculated values because of diffusion of ions with different concentrations, change of the conductivity of the electrolyte and the pH by reduction of protons, and generation of very small bubble on the surface of the electrode following molecular hydrogen or oxygen formation. For instance, the effectiveness of 90° pulses can vary from the optimal value providing the maximum intensity and decrease the peak areas representing the concentrations of the electrolytes. The NMR signal intensity, which is proportional to the probe quality factor Q, can vary also with the change of the conductance of the electrolyte, because highly conducting samples (salt solutions) can dampen the quality factor Q and affect proper tuning and matching. Therefore, the external standard in an isolated capillary tube is used as an *in situ* probe to monitor the variation in the conditions, and then the concentrations of the other compounds in the same conditions can be amended. The blue and red solid circles in Fig. 8 show the trends of the corrected concentrations of the EC reactants based on the peak area of benzene.

IV. CONCLUSION

A three-electrode EC cell based on a PGF working electrode has been constructed and its EC and *in situ* qNMR performances have been investigated in a standard 5 mm NMR probe by simultaneously acquiring EC signals and high-resolution NMR spectra. The PGF device has the advantage of reducing the interference of the RF, which has the potential to increase the sensitivity in NMR detection. Evolution of *in situ* EC-qNMR spectrum monitoring of redox of *p*-benzoquinone and hydroquinone with time shows the feasibility of the EC-NMR cell. In addition to giving structural information

about the intermediate and product based on their chemical shifts, EC reaction monitoring and kinetic analysis can be achieved by the EC-NMR cell, showing its suitability for simultaneous qualitative and quantitative analysis.

SUPPLEMENTARY MATERIAL

See supplementary material for the theoretical analysis of the shielding effect of the thin film in an alternative magnetic field, the magnetic field shielding in different metal film cylinders (Fig. S1), the absolute content method for quantitative content determination in EC-NMR, measurement of the volume ratio of the NMR tube relative to the coaxial capillary (Table S1), and the precision and accuracy of the quantitative method (Table S2).

ACKNOWLEDGMENTS

This work was supported by The National Natural Science Foundation of China (21327001 and 21505109) and the Fundamental Research Funds for Central Universities (20720160074, 20720160125, and 20720150109).

[1] J. M. Griffin, A. C. Forse, W. Y. Tsai, P. L. Taberna, P. Simon, and C. P. Grey, Nat. Mater. **14**, 812 (2015).
[2] F. Poli, A. Wong, J. S. Kshetrimayum, L. Monconduit, and M. Letellier, ACS Chem. Mater. **28**, 1787 (2016).
[3] R. Boisseau, U. Bussy, P. Giraudeau, and M. Boujtita, Anal. Chem. **87**, 372 (2015).
[4] Z. Wu, C. S. Wu, P. J. Chu, and S. Ding, Magn. Reson. Imag. **27**, 871 (2009).
[5] J. A. Tang, G. Zhong, S. Dugar, J. A. Kitchen, Y. Yang, and R. Fu, J. Magn. Reson. **225**, 93 (2012).
[6] C. Li, X. Lou, M. Shen, X. Hu, Z. Guo, Y. Wang, B. Hu, and Q. Chen, ACS Appl. Mater. Interfaces **8**, 15352 (2016).
[7] X. Zhang and J. W. Zwanziger, J. Magn. Reson. **208**, 136 (2011).
[8] Z. R. Ni, X. H. Cui, S. G. Sun, and Z. Chen, Spectrosc. Spect. Anal. **31**, 1 (2011).
[9] L. Huang, J. Y. Sun, S. H. Cao, Z. R. Ni, Z. Chen, and S. G. Sun, ACS Catal. **6**, 7686 (2016).
[10] F. Schauer, L. Tkáč, M. Ožvoldová, V. Nádaždy, K. Gmucová *et al.*, AIP. ADV. **7**, 055002 (2017).
[11] J. Li, X. Qi, G. Hao, L. Ren, and J. Zhong, AIP ADV. **5**, 067154 (2015).
[12] D. I. Hoult, Concept. Magnetic Res. **12**, 173 (2000).
[13] S. Klod, F. Ziegs, and L. Dunsch, Anal. Chem. **81**, 10262 (2009).
[14] J. A. Richards and D. H. Evans, Anal. Chem. **47**, 964 (1997).
[15] K. Albert, E. L. Dreher, H. Straub, and A. Rieker, Magn. Reson. Chem. **25**, 919 (1987).
[16] D. W. Mincey, M. J. Popovich, P. J. Faustino, M. M. Hurst, and J. A. Caruso, Anal. Chem. **62**, 1197 (1990).
[17] M. E. Sandifer, M. Zhao, S. Kim, and D. A. Scherson, Anal. Chem. **65**, 2093 (1993).
[18] P. D. Prenzler, R. Bramley, S. R. Downing, and G. A. Heath, Electrochem. Commun. **2**, 516 (2000).
[19] R. D. Webster, Anal. Chem. **76**, 1603 (2004).
[20] G. Frens, Nature Phys. Sci. **241**, 20 (1973).
[21] J. A. Stratton, *Electromagnetic theory* (Wiley-IEEE press, 2007).